Journal of Geosciences and Geomatics, 2025, Vol. 13, No. 2, 31-43
Available online at http://pubs.sciepub.com/jgg/13/2/1
Published by Science and Education Publishing
DOI:10.12691/jgg-13-2-1

Geochemistry and ^{40}ar/^{39}ar Geochronology of Amphibolites from Banefo-Mvoutsaha Area, Central Domain of the Pan-African Fold Belt in Cameroon

MVODO Hermine[1], NGA ESSOMBA TSOUNGUI Philomène Estelle[2], KOUANKAP NONO Gus Djibril[3,*], KAMGUIA WOGUIA Brice[4], SIMO Pascal[4]

[1]Departement of Geosciences and Environnement, University of Ebolowa, P.O.Box 118 Ebolowa, Cameroon
[2]Department of Mining Engineering and Mineral Processing, National Advanced School of Mines and Petroleum Industries, University of Maroua, P.O.Box 46 Maroua, Cameroon
[3]Department of Geology, HTTC, University of Bamenda, P.O.Box 39 Bambili; Bamenda, Cameroon
[4]Laboratory of Petrology and Structural Geology, University of Yaoundé I, PO Box 3412 Messa-Yaoundé, Cameroon
*Corresponding author: kouankap@yahoo.fr

Received June 05, 2025; Revised July 07, 2025; Accepted July 14, 2025

Abstract The Banefo-Mvoutsaha area lies along the Central Cameroon Shear Zone and belongs to the Central Domain of the Pan-African Fold Belt in Cameroon. The amphibolites of the study area are of two types: The banded amphibolites which are associated with migmatites and composed of Hbl + Bt + Qtz + Kfs + Pl ± Grt + Op; and the massive amphibolites which outcrops as discontinuous bands within the garnet bearing-gneisses; its mineral assemblage is made up of Hbl + Qtz + Kfs ± Grt ± Op. The studied amphibolites are ortho-derived, their SiO_2 contents range from 48 to 52 wt%, they are enriched in LREEs and LILEs relatively to HREE, and display negative Eu anomalies ($0.65 \leq Eu/Eu^* \leq 0.96$), characteristics of alkali basaltic rocks, which belong to intraplate tholeiitic series. The banded amphibolites samples yield an Ar-Ar age of 618.14 ± 11.43 Ma, while the massive amphibolites samples ages are 547.50 ± 3.15 Ma. The 618 Ma age coincide with the emplacement age of granitoids that intruded the metamorphic basement of the area. The age of 547.50 ± 3.15 Ma is correlated to amphibolitic metamorphism events that mark the end of the Pan-African orogeny in the study area. These new Ar-Ar ages therefore point out at least two phases of amphibolitic metamorphism in the Central domain of the Pan-African Fold Belt in Cameroon.

Keywords: *Pan-African, Amphibolite, Tholeiites series, Intraplate basalts, Argon-Argon*

Cite This Article: MVODO Hermine, NGA ESSOMBA TSOUNGUI Philomène Estelle, KOUANKAP NONO Gus Djibril, KAMGUIA WOGUIA Brice, and SIMO Pascal, "Geochemistry and ^{40}ar/^{39}ar Geochronology of Amphibolites from Banefo-Mvoutsaha Area, Central Domain of the Pan-African Fold Belt in Cameroon." *Journal of Geosciences and Geomatics*, vol. 13, no. 2 (2025): 31-43. doi: 10.12691/jgg-13-2-1.

1. Introduction

Collisional orogenic belts are worldwide associated to amphibolitic metamorphic facies from medium to high grades [1,2,3,4]. Amphibolites are therefore used to characterize orogenies which help: 1) to reveal the nature of the parent rocks; 2) to constraint the different tectonic setting and metamorphism phases; 3) and to time the tectono-metamorphism events [5,6,7]. The panafrican orogeny formations in Cameroon (Figure 1) are made up of wide range of magmatic and metamorphic rocks, including amphibolites of various metamorphic grades and ages [8,9,10,11]. The Banefo-Mvoutsaha area located in the southern part of the Cameroon Central Shear Zone comprises metamorphic rocks intruded by granitic plutons (Figure 2). The Banefo-Mvoutsaha granitoid massif is made up of syn- to post-tectonic, high-K calc-alkaline rocks showing chemical composition of granite, quartz-monzonite and granodiorite [12]. Geochronological data from U-Pb zircon dating yielded an age of 602 ± 1.4 Ma for the coarse-grained meta-granites [13]. These granitic bodies are elongated N70°E and were emplaced during and after the D_2 deformation phase along the Cameroon Central Shear Zone (CCSZ). Amphibolites outcrop in Bafeno-Mvoutsaha area and are still poorly investigated [14]. In this paper we present the whole rock geochemical data and the $^{40}Ar/^{39}Ar$ geochronology data of the amphibolites from the study area to constraint their protoliths, the geotectonic setting and the ages of amphibolitic metamorphism in the Pan-African Fold Belt in Cameroon.

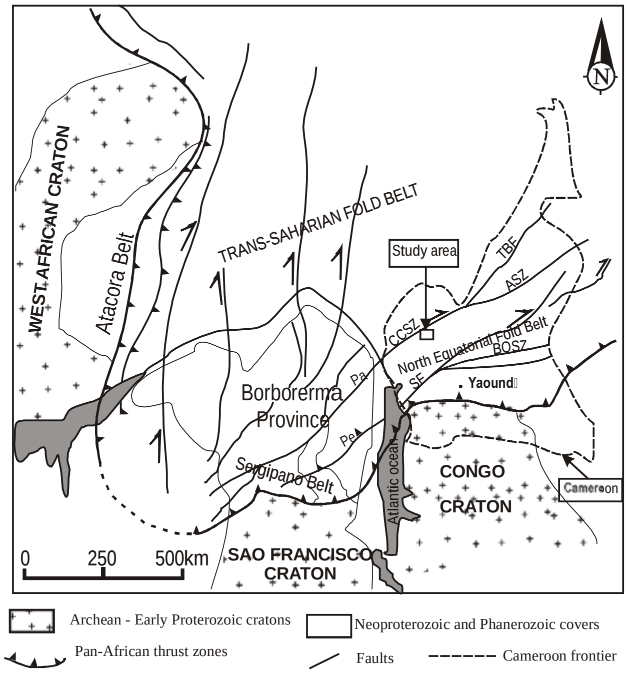

Figure 1. Geological reconstruction of African Panafrican domains and NE Brazil showing the continuity of the Sergipano Belt and North Equatorial Fold Belt [modified After 15,16,18,19]. **ASZ**: Adamawa shear zone; **CCSZ**: Central Cameroon Shear Zone; **BOSZ**: Bétaré-Oya shear zone; **Pe**: Pernambuco shear zone; **Pa**: Patos shear zone **SF**: Sanaga Fault; **TBF**: Tibati-Banyo Fault. Dash lines represent the boundary of Cameroon

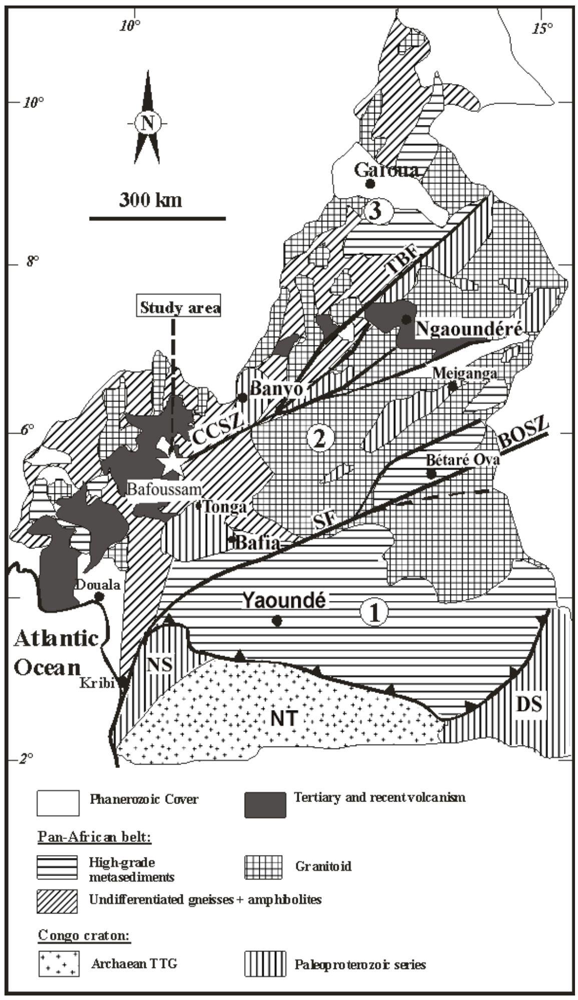

Figure 2. Geological map of Cameroon with the three main domains of the Pan-African North-Equatorial Fold Belt [modified After 15], (**1**) southern domain corresponding to the Yaoundé series thrust on the Congo Craton, (**2**) central domain, (**3**) northern domain; granitoids suites are not further distinguished. **CCSZ**: Central Cameroon Shear Zone; **DS**: Dja series; **NS**: Nyong series; **NT**: Ntem complex; **SF**: Sanaga Fault; **TBF**: Tibati-Banyo Fault. Location of study area is marked by a star

2. Geological Setting

The Neoproterozoic belt in Cameroon is widely known as the Pan-African North Equatorial Fold Belt (PANEFB) [15,16]. This belt is a prolongation in the African continent of the Braziliano-Panafrican Belt in South America across the Atlantic (Figure 1) [17,18,19]. In Cameroon, the Neoproterozoic belt is made up of three distinct geodynamic domains [20,21,22,23,24]: the northern domain and the southern domain which are separated by the central domain (Figure 2).

The northern domain consists of restricted 830 Ma metavolcanic rocks of tholeiitic and alkaline affinities associated with metasediments and widespread 630-660 Ma calc-alkaline orthogneisses whose age is interpreted as a major episode of continental accretion [25]. A Paleoproterozoic crustal source in this region is attested by the presence of 2 Ga old inherited zircons in the granitoids within the orthogneisses [25].

The southern domain comprises Neoproterozoic metasedimentary units such as the Yaoundé, Mbalmayo and Ntui-Betamba series. The protoliths of these units were deposited in a passive margin environment at the northern edge of the Congo Craton, and were metamorphosed under high-P conditions (T = 750-800°C, P = 9-13Kb) at 616 Ma [15,23]. A Pan-African meta-igneous rock assemblage comprising alkaline ultramafic to metagabbros and amphibole-bearing alkaline orthogneisses [23] was also recognized in association with these Neoproterozoic units. The rocks of this southern domain were thrusted onto the Archean Congo Craton towards the south [26].

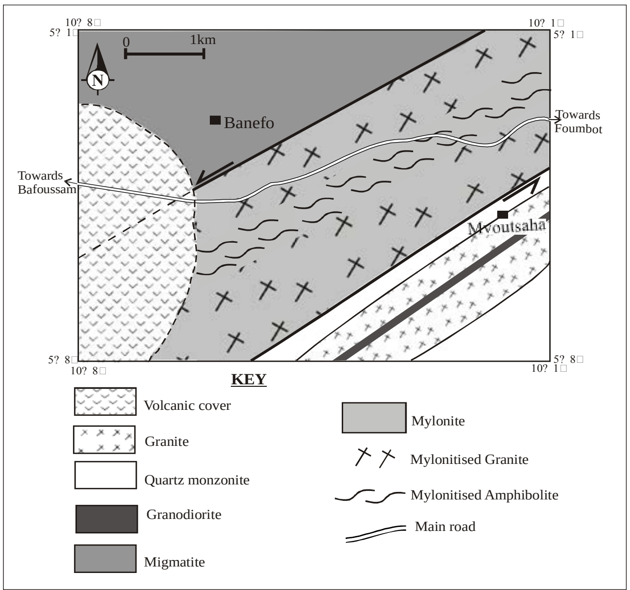

Figure 3. Geological map of the Banefo-Mvoutsaha massif [modified after 12] showing sample locations

The central domain in which the present study area is located (Figure 2, Figure 3) is situated between the Sanaga fault to the South and the Tibati-Banyo fault to the North [27]. The metamorphic basement of the central domain consists of an assembly of fragments of Paleoproterozoic continental crust, recrystallized under high-grade granulite facies (850-900°C, 10-12Kb) at ca 2100 Ma, and associated with Neoproterozoic amphibolite and gneiss [5,8,22,24]. This basement is intruded by widespread Neoproterozoic syntectonic plutonic rocks of high-K, calc-alkaline affinities [12,13,20,21,24,28,29,30,31,32,33]. In the central domain polycyclic metamorphism and three phases of deformation related to metamorphic recrystallisation under low to high grade amphibolite facies conditions have been identified.

3. Analytical Methods

Fresh representative samples were sent to ACME Analytical Laboratories Ltd, Vancouver, Canada for whole rock geochemical analysis. Whole rock analyses for major and trace elements were carried out by Inductively-Coupled Plasma Mass Spectrometry (ICP-MS) from pulps. 0.2g of rock powder was fused with 1.5g LiBO2 and then dissolved in 100MM3 5%HNO3. The REE contents were determined by ICP-MS from pulps after 0.25g rock-powder was dissolved with 4 acid digestions. Analytical uncertainties vary from 0.1% to 0.04% for major elements; from 0.1 to 0.5% for trace elements; and from 0.01 to 0.5ppm for rare earth elements.

The Ar-Ar geochronology was performed at the Department of Isotope Geochemistry, Vrije Universiteit de Boelelaan, Amsterdam, The Netherlands. For the two samples (T21G9 and T22A) of amphibolites, hornblende grains measuring as 400-500 microns were used. The $^{40}Ar/^{39}Ar$ measurements were accomplished on an MAP-215-50 mass spectrometer in VU University Amsterdam. The experimental methods follow those developed at Amsterdam by [34].

4. Results

4.1. Petrography

The amphibolites investigated in Banefo-Mvoutsaha area are subdivided, based on their field occurrences and structure into two types. The first one is massive and outcrops as centimetric and discontinuous bands (Figure 4A). The second type is the banded amphibolites which is interbedded with migmatitic gneisses and garnet gneisses (Figure 4E). Those bands are parallel to the foliation within the garnet-bearing gneisses.

4.1.1. Massive Amphibolites

The massive amphibolites are very fine to fine grained. They are dark green in color and show poorly-developed foliation (Figure 4A). They occur within garnet-gneisses as lenses of 30 cm - 5 m long and 10 - 20 cm width. It is no easy to see minerals with necked eye, while in microscope, the rock displays granolepidoblastic heterogranular microstructure comprising amphibole, quartz, feldspar, pyroxene, rutile and opaque minerals which are preferentially oriented following the same direction. Amphibole crystals which are the most abundant minerals, are fish-amphibole according to their form (Figure 4B). Depending on their color, two types of amphibole crystals are observed: greenish-light (Figure 4C) and brownish crystals (Figure 4D). The brownish amphibole crystals are secondary resulting from destabilization of pyroxene. Some of these minerals contain opaque minerals inclusions. Quartz and feldspar fill the interstices between amphibole crystals following the same direction as amphibole fish crystals (Figure 4B, Figure 4C). Garnet is very low in the rock, as well as pyroxene crystals, which destabilizes into amphibole crystal. They also follow the same orientation as amphibole, quartz and feldspar. The accessory phase is made of opaque minerals and rutile. Opaque minerals are anhedral primary and secondary minerals (Figure 4B). Mineral assemblages are Hbl + Qtz + Kfs + Px ± Grt ± Op (primary assemblage) and Hbl + Px ± Op (secondary assemblage). They are respectively characteristics of high-grade and low-grade amphibolite facies.

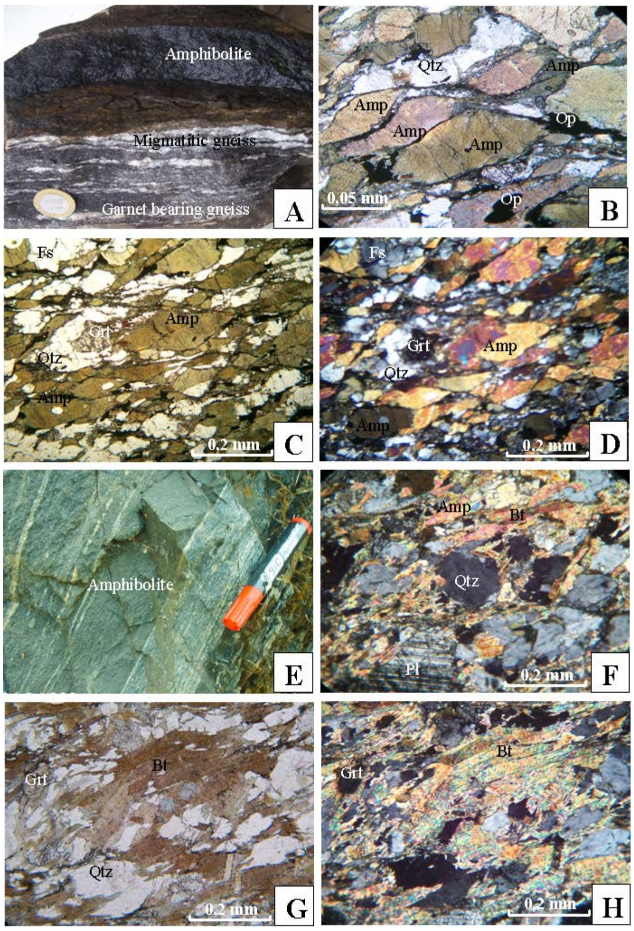

Figure 4. Photographs and micrographs of Banefo-Mvoutsaha amphibolites. A) Occurrence of massive amphibolites interbedded with migmatitic gneisses and garnet-bearing gneisses. B) heterogranular granolepidoblastic texture. Noted the orientation of the minerals and the presence of amphibole-fish. C) LPNA micrograph showing oriented amphibole, quart, garnet and pyroxene. D) LPA micrograph showing destabilization of pyroxene into brownish amphibole. E) Occurrence of banded amphibolites. Note the foliation. F) Granoblastic heterogranular texture. Quartz is rounded. Stocky and subhedral plagioclase crystals. G) LPNA micrograph showing a pile of biotite flake. H) LPA micrograph

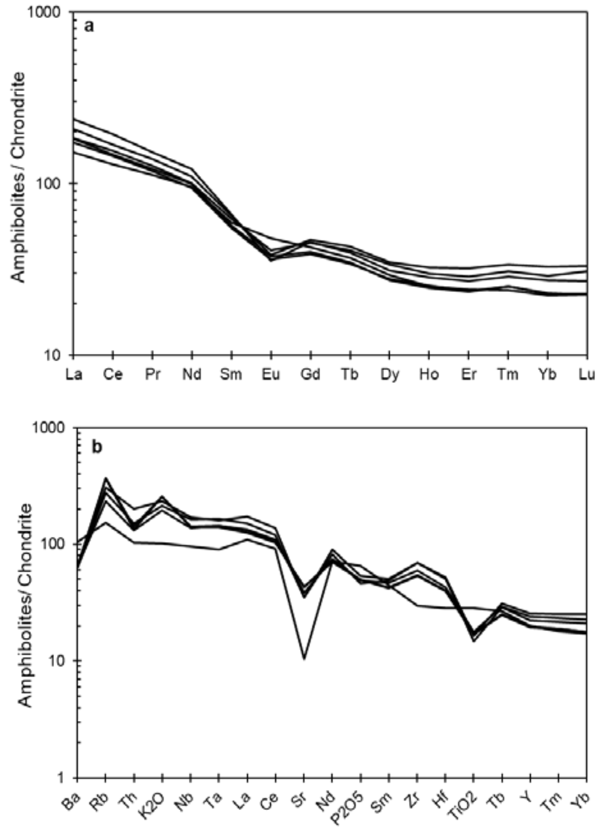

Figure 5. A) Chondrite normalized REE distribution diagram for the Banefo-Mvoutsaha amphibolites. The normalizing chondrite values are from [35]. B) Primitive mantle-normalized multi-element patterns. The normalizing chondrite values are from [36]

4.1.2. Banded Amphibolites

The banded amphibolites are greyish in color. As well as the massive amphibolites, they display very fine to fine grain. The foliation is more expressive (Figure 4E), and the alternance of quartzo-feldspathic bands and ferromagnesian bands is clearly observed. The rock is intimately associated with migmatites. In thin section, the rock displays a granoblastic heterogranular texture consisting of quartz, biotite, amphibole, feldspar, garnet and plagioclase (Figure 4F). Minerals are poorly deformed, differently from the massive amphibolites. Quartz and biotite are the most abundant minerals in this rock. Quartz is mostly rounded (Figure 4E), occurring as anhedral mineral (Figure 4F). Biotite flakes are primary minerals and are scattered in the rock. Amphiboles are anhedral and primary minerals. The percentage of the garnet is lower than in the other rock. Stocky plagioclase crystals are subhedral and lurking in the matrix. The mineral assemblage is made of Hbl + Bt + Qtz + Kfs + Pl ± Grt + Op Which is characteristic of low-grade amphibolite facies. Along micro-shear planes in the study area, the banded amphibolites have been deformed into ultramylonites and pseudotachylites fault rocks.

4.2. Whole Rock Geochemistry

Seven fresh samples of amphibolites (massive and banded) were collected and analyzed for whole-rock majors and trace elements, and their compositions are listed in Table 1.

Table 1. Geochemical data of selected samples of amphibolites from Banefo-Mvoutsaha area. Analyses performed at Acme lab, Vancouver, CANADA

Rocks type		T22A2	T22A3	T22A5A	T21G9	TAIF	TA1
	MDL						
Wgt	0.01	0.28	0.58	0.25	0.41	0.48	0.39
SiO_2	0.01	49.88	48.59	48.98	48.35	51.13	50.69
Al_2O_3	0.01	17.25	16.36	16.67	13.86	17.12	17
Fe_2O_3	0.01	12.43	11.42	11.27	16.15	12.11	10.53
MgO	0.01	3.32	5.69	5.32	4.28	2.86	4.38
CaO	0.01	5.57	6.13	5.66	9.3	4.93	5.36
Na_2O	0.01	5.03	3.92	4.06	1.79	5.25	4.97
K_2O	0.01	2.8	3.67	3.67	1.47	3.06	3.39
TiO_2	0.01	1.84	1.78	1.74	2.94	1.69	1.52
P_2O_5	0.001	0.515	0.526	0.522	0.683	0.487	0.561
MnO	0.01	0.19	0.16	0.16	0.27	0.19	0.16
Cr_2O_3	0.002	0.002	0.021	0.02	0.006	<0.002	0.016
Sum	0.01	99.71	99.67	99.68	99.69	99.73	99.69
LOI	-5.1	0.9	1.4	1.6	0.6	0.9	1.1
Ni	20	<20	79	82	<20	<20	53
Sc	1	18	21	20	37	15	17
Ba	1	442	438	448	721	436	463
Be	1	4	3	3	<1	4	3
Co	0.2	30	35.4	33.3	38.6	25.6	26.2
Cs	0.1	1	3.4	3	0.6	1.3	2.7
Ga	0.5	22.8	18.3	18.7	19.2	23.2	20.3
Hf	0.1	8.6	8.1	7.9	5.7	10.4	10.1
Nb	0.1	48.3	49.9	48.9	33.7	57.1	59.7
Rb	0.1	81.6	128.2	129.6	53.6	96.6	106.9
Sn	1	4	4	4	2	3	3
Sr	0.5	453.1	505.8	515.1	122.2	416.4	417.3
Ta	0.1	2.9	2.9	2.8	1.8	3.3	3.2
Th	0.2	5.5	5.6	6	4.3	6.3	8.4
U	0.1	1.5	1.5	1.4	0.8	1.8	2
V	8	64	99	91	302	46	77
W	0.5	<0.5	0.6	<0.5	<0.5	<0.5	<0.5
Zr	0.1	409.4	372.5	369.1	204.1	474.7	473.7
Y	0.1	48.1	39.2	39	40.2	50.8	44.4
La	0.1	43.5	43.4	41.1	35.9	49.2	56.4
Ce	0.1	95.1	90.6	88.6	79.2	103.1	118.2
Pr	0.02	12.04	11.54	11.21	10.71	13.16	14.51
Nd	0.3	47.1	46.6	44.2	44.8	51.6	56.8
Sm	0.05	9.56	8.72	8.49	9.1	9.97	10.21
Eu	0.02	2.38	2.19	2.11	2.79	2.23	2.06
Gd	0.05	9.29	8.22	7.97	8.78	9.64	9.36
Tb	0.01	1.53	1.3	1.28	1.38	1.61	1.49
Dy	0.05	8.55	6.95	7.09	7.44	8.86	7.91
Ho	0.02	1.7	1.39	1.44	1.43	1.84	1.61
Er	0.03	4.74	3.88	3.94	4.02	5.29	4.49
Tm	0.01	0.79	0.64	0.64	0.61	0.86	0.73
Yb	0.05	4.95	3.9	3.88	3.81	5.55	4.62
Lu	0.01	0.78	0.57	0.58	0.57	0.84	0.69
C/TOT	0.02	0.11	0.04	0.11	0.06	0.11	0.04
Mo	0.1	2.7	3.5	4	1.6	7	4.6
Cu	0.1	48.5	58.9	53.5	129.5	36.1	27.7
Pb	0.1	2	3.4	4.5	1.2	2.6	3.9
Zn	1	99	78	89	58	120	86
Ni	0.1	11.1	80.2	87.4	10.8	8.6	56.3
As	0.5	<0.5	<0.5	<0.5	<0.5	0.7	<0.5
Cd	0.1	0.2	<0.1	0.1	<0.1	0.1	0.1

Rocks type		T22A2	T22A3	T22A5A	T21G9	TAIF	TA1
Sb	0.1	<0.1	<0.1	<0.1	<0.1	<0.1	<0.1
Bi	0.1	<0.1	<0.1	<0.1	<0.1	<0.1	<0.1
Ag	0.1	<0.1	<0.1	<0.1	<0.1	<0.1	<0.1
Au	0.5	1.8	0.8	<0.5	0.8	1	0.8
Hg	0.01	<0.01	<0.01	<0.01	<0.01	<0.01	<0.01
Tl	0.1	0.5	0.7	0.6	0.3	0.5	0.6
Se	0.5	0.6	<0.5	<0.5	<0.5	0.9	0.5
CNK		13.4	13.72	13.39	12.56	13.24	13.72
A/CNK		1.29	1.19	1.24	1.10	1.29	1.24
NK		7.83	7.59	7.73	3.26	8.31	8.36
A/NK		2.20	2.16	2.16	4.25	2.06	2.03
La/Yb		8.79	11.64	12.16	9.42	8.86	11.77
Nb/Ta		16.66	17.21	17.46	18.72	17.30	18.66
Zr/Sm		42.82	42.72	43.47	22.43	47.61	46.40
La/Nb		0.90	0.91	0.84	1.07	0.86	0.91
La/Ta		15.00	15.66	14.68	19.94	14.91	17.00
Th/Yb		1.11	1.44	1.78	1.13	1.14	1.82
Eu/Eu*		0.78	0.80	0.79	0.96	0.70	0.65
$(La/Yb)_N$		5.78	7.32	6.97	6.20	5.83	8.03
$(Gd/Yb)_N$		1.50	1.69	1.65	1.85	1.39	1.62
$(Gd/Lu)_N$		1.48	1.80	1.71	1.92	1.43	1.69
$(La/Sm)_N$		2.77	3.03	2.95	2.40	3.00	3.36

Table 2. Summary of Ar-Ar geochronology data of samples T21G9 and T22A

Sample codes	VU82-C9	T21G9	VU82-C10	T22A
AGE	547.50		618.14	
2-Sigma	± 3.15	± 0.58%	± 11.43	± 1.85%
MSWD	65.03		569.80	
%. n in plateau	99.68	21	72.20	11
K/Ca	0.177		0.125	
2-sigma	± 0.016		± 0.004	
intercept	330.4279		539.2708	
2-sigma	± 40.7680	± 12.34%	± 222.6103	± 41.28%
isochron age	546.42		594.63	
2-Sigma	± 3.41	± 0.62%	± 25.23	± 4.24%
MSWD	59.18		> 100	
$^{40}Ar/^{39}Ar$	110.8005		127.7045	
2-Sigma	± 0.5913	± 0.53%	± 2.7407	± 2.15%

4.2.1. Major Elements

Amphibolite samples are characterized by SiO_2 content ranging between 48 wt% and 52 wt%. The percentage of Al_2O_3 is high (16.36 – 17.25 wt%), except for the sample T21G9 which shows a relatively low percentage (13.86 wt%). As well as Al_2O_3, samples show low Fe_2O_3 values (10.53 – 12.43 wt%), while the T21G9 sample displays 16.15 wt% value. The rock present low values of MgO (2.86 – 5.69 wt%) and CaO (4.93 – 6.13 wt%), except for T21G9 sample (9.30 wt% for CaO). TiO_2 contents range from 1.52 wt% to 2.94 wt%. The averages A/CNK molar (Al_2O_3/ CaO + Na_2O + K_2O), and A/NK molar (Al_2O_3/ Na_2O + K_2O) values are 1.22 and 2.47 respectively.

4.2.2. Trace Elements

The Banefo-Mvoutsaha amphibolites sample display variable high field strength elements (HFSE: e.g Nb, Ta, Zr, Hf) and large-ion-lithophile elements (LILE; e.g., Ba, Rb, K and Sr) concentrations (Table 1). Ba concentrations are from 436 to 721ppm, Rb (59.6 – 109.6ppm), and Sr from 122.2 to 515.1 ppm.

Samples are enriched in LILE (Rb, K), and relatively weakly depleted in the other elements. On the chondrite-normalized rare earth element (REE) diagram from [35], all the samples REE pattern are weakly fractionated (La_N/Yb_N= 5.78 – 8.03) marked by a slight enrichment of LREE patterns (La_N/Sm_N = 2.40 – 3.36) relatively to HREE (Gd_N/Yb_N= 1.39 – 1.85). The samples display a negative Eu anomaly with Eu/Eu* ratio values ranging between 0.65 and 0.96 (Figure 5A), which highlight feldspar fractionation in the rock, confirmed by the negative anomalies on Sr. On the multi-elements chondrite-normalized plots from [36], Rb, K, Nd and Zr show positive anomalies, and Th, Sr and Ti display negative anomalies except for the sample T21G9 (Figure 5B).

4.3. Ar-Ar Geochronology

The summary of Ar-Ar geochronology data is represented in Table 2. Two representative samples from the massive amphibolites (T21G9) and the banded amphibolites (T22A) have been subjected to dating.

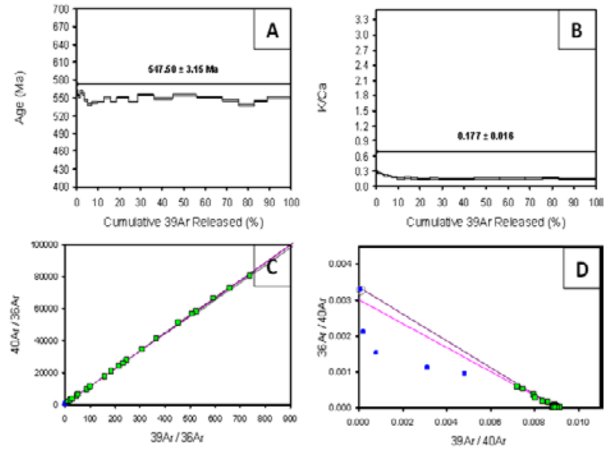

Figure 6. Graphic representations of Ar-Ar data of massive amphibolites sample (T21G9): (A and B) patterns of cumulative 39Ar released %, (C and D) normal and inverse isochrons respectively)

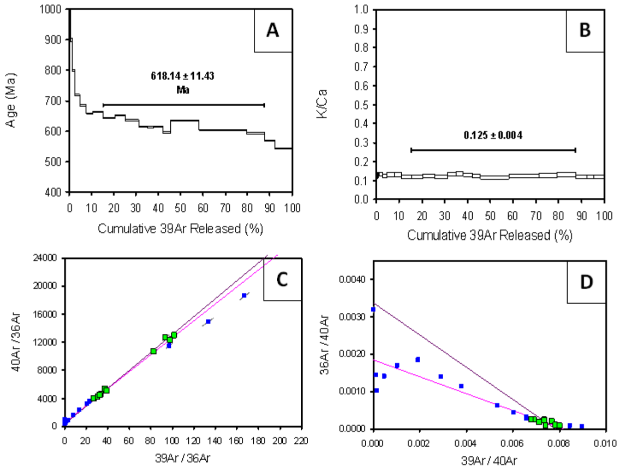

Figure 7. Graphic representations of Ar-Ar data of banded amphibolites sample (T22A): (A and B) patterns of cumulative 39Ar released %, (C and D) normal and inverse isochrons respectively)

The results of Ar release during stepwise heating and inverse isochrones are given on Figures 6 and 7 for T21G9 and T22A respectively. Sample T21G9 yield an Ar-Ar age of 547.50 ± 3.15 Ma (Figure 6A), the patterns of cumulative ^{39}Ar released %, are relatively flat, and constant from 10% to 100% ^{39}Ar released (Figure 6B). Sample T22A yielded an Ar-Ar age of 618.14 ± 11.43 Ma (Figure 7A), the patterns of cumulative ^{39}Ar released %, show a significant variation in the age plateau, and the results of this sample do not give a line in various isochron diagrams, variation of loss and gain ^{39}Ar released is noted (Figure 7B). Data from T21G9 crushing experiments in $^{39}Ar/^{36}Ar$ vs. $^{40}Ar/^{36}Ar$ diagram define a homogenous line on the normal isochron for massive amphibolites samples (Figure 6C), but show a disparity line for the banded amphibolites. From 0 to 60 for $^{40}Ar/^{36}Ar$ values, the line is homogen, and the disparity start from 70 up to 200 for $^{40}Ar/^{36}Ar$ values (Figure 7C). In the inverse isochron diagram, the difference is considerable between the two amphibolites. The results of the apparent age spectrum plots for these stepwise-crushing experiments are presented in $^{36}Ar/^{40}Ar$ vs. $^{39}Ar/^{40}Ar$ diagrams (Figures 6D and 7D). The lines are not homogeneous, but the gap is wider in the banded amphibolites (Figure 7D). The $^{36}Ar/^{40}Ar$ values range from 0.0020 to 0.0030 above, while for T21G9 sample, the gap is slight and the lines are very close (Figure 6D). The age spectrum is a convenient way to present the data in terms of progressive gas release [34]. It should be noted that the gas is released by progressive crushing and not by progressive heating as it is more commonly the case in $^{40}Ar/^{39}Ar$ dating experiments.

5. Interpretation and Discussion

5.1. Petrogenesis of Banefo-Mvoutsaha Amphibolites

The positions of studied amphibolites are shown in the TiO_2-Ni discriminating diagram for ortho and para amphibolites of [37] and the Zr/TiO_2 vs Ni diagram indicate that they are orthoderived, with an igneous source for the parental rocks (Figures 8A and 8B). The same results are described in the center domain of CAFB in Makénéné [5], the Fomopéa pluton [11], in Kombé II [8], and in the Congo craton from Akom II [38], Mewongo [7], and Toko-Nlonkeng [39] areas. The geochemical classification of extrusive rocks diagram using Nb/Y vs. Zr/Ti adapted from [40] shows the volcanic origin of those rocks (Figure 8C), where the main samples plot in alkali-basalts field, except one sample falling within the basalts field, probably due to some contamination of the magma source. Alkali basalts are characterized by highest Na_2O and K_2O content than the basic basalts, and low SiO_2 contents (48.35 – 51.13 wt%) [41,42], they are located behind the arc. However, they are not likely to form at depths shallower than 50-60 km [43,44]. This hypothesis is confirmed by the high values in Ni (11 – 87.4 ppm) and Co (25.6 – 38.6 ppm) which are evidence of a (deep) mantle source [45]. Amphibole and rutile as residual minerals can be used to constrain this source. Indeed, rutile and amphibole are index minerals which usually contain abundant Nb and Ta. In the rutile mineral composition, Ta is relative to Nb, and the experimental results showed that, if minor rutile appears in the residual source, the Nb/Ta ratios in the coexisting partial melts will increase [46]. On the other hand, Nb is more compatible than Ta in amphibole and small amount of amphibole as residual mineral could lead to lower Nb/Ta ratios [46]. All samples of massive and banded amphibolites display lower Nb/Ta ratios (16.65 – 18.72), indicating the compositional source of amphibole minerals.

The degree of contamination can be estimate through certain chemical parameters. For example, the major elements TiO_2 is a well-founded discrimination between arc and spreading ridge basalts [47, 48]. He is relatively immobile during alteration. Low TiO_2 content suggests that the protolith is in an arc system [47]. But the TiO_2 content of the study amphibolites is low to medium (1.52 – 2.94 wt%), this needs others explanations to give a conclusion. In the same vein, ratios of some trace elements can constrain the crustal contamination in basaltic rocks. Those which are affected by crustal contamination exhibit La/Ta = 22 and La/Nb = 1.5 [49]. The studied amphibolites display low values of La/Ta and

La/Nb, respectively ranging from 14.9 – 19.9 and 0.84 – 1.06, and this confirm that the role of contamination during magma evolution has been minimal. In addition, incompatible trace elements such as Ta, Yb and Th are considered to determine crustal contamination. The crustal contamination affects Th more than Ta and Yb. The contamination shows high Th/Yb values [50]. The studied amphibolites show low values of Th/Yb (1.1 – 1.8), and this suggests no or minimal crustal contamination for Banefo-Mvoutsaha amphibolites parent rocks.

Furthermore, the fractionation occurs during the formation of the protoliths of those amphibolites. The REE patterns are marked by TiO_2, Sr and Eu anomalies (Figure 5). The TiO_2 anomaly in multi-element diagram suggests a Ti-oxides fractionation. The Sr anomaly in multi-element diagrams indicates plagioclase fractionation [51]. This fractionation of plagioclase is confirmed by the presence of Eu anomaly (Eu/Eu*: 0.65 – 0.96) in the chondrite normalized REE diagrams of Banefo-Mvoutsaha amphibolites, which indicate a plagioclase-depleted crustal source or fractionation during magmatic differentiation. The $K_2O + Na_2O$ vs. $K_2O/(K_2O+Na_2O)$ diagram [52] displays an assimilation and fractional crystallization trend (Figure 9). We can see through this plot, the role of the fractionation in the rock's emplacement. The combination between low MgO value and moderate to high Fe_2O_3 contents also suggest fractional crystallization, but the fractional crystallization of Mg-rich minerals (i.e., pyroxene) which is typical of tholeiitic magmas [53]. In the same way, the parental basaltic magma from which the Banefo-Mvoutsaha amphibolites were derived is inferred to belong to the tholeiitic series as shown by the SiO_2 vs. FeOt/MgO diagram (Figure 10) of [54], like in the Mewongo area [7]. All the samples of Banefo-Mvoutsaha amphibolites plot in the tholeiitic series area and display a tholeiitic trend as demonstrated in the Mg# vs. SiO_2/Al_2O_3 diagram, showing the primitive basalts field and differentiation [55] and mineral fractionation trends (Figure 11) adapted after [56].

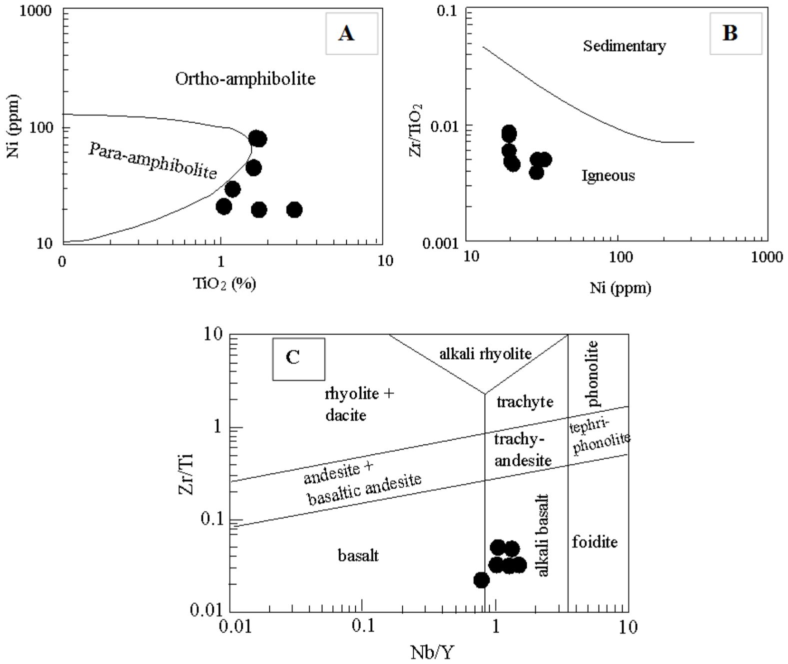

Figure 8. Geochemical classification diagrams of Banefo-Mvoutsaha amphibolites. **A)** Studied amphibolites position in the TiO_2-Ni discriminating diagram for Ortho and para-amphibolites [37]. **B)** Zr/TiO_2/Ni plot diagram of metavolcanic rocks [from 36]. **C)** Zr/Ti vs. Nb/Y Plot of amphibolites protolites [40]

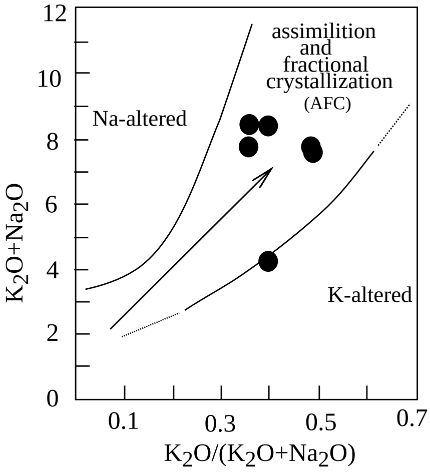

Figure 9. K_2O+Na_2O vs. $K_2O/(K_2O+Na_2O)$ diagram of igneous rocks [adapted from 52] showing alteration trend of Bafoussam amphibolites

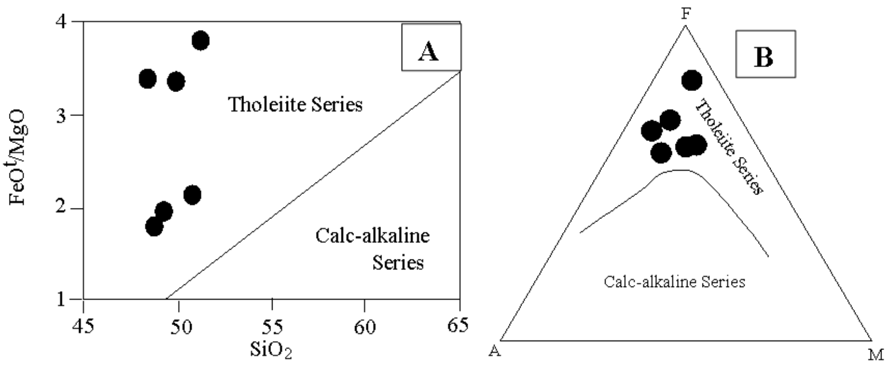

Figure 10. Discrimination diagrams showing the affinity of Banefo-Mvoutsaha amphibolites. A) FeOt/MgO vs. SiO_2 Plot of [54]. B) The AFM discrimination plot [70] showing tholeiitic affinity of the Bafoussam amphibolites

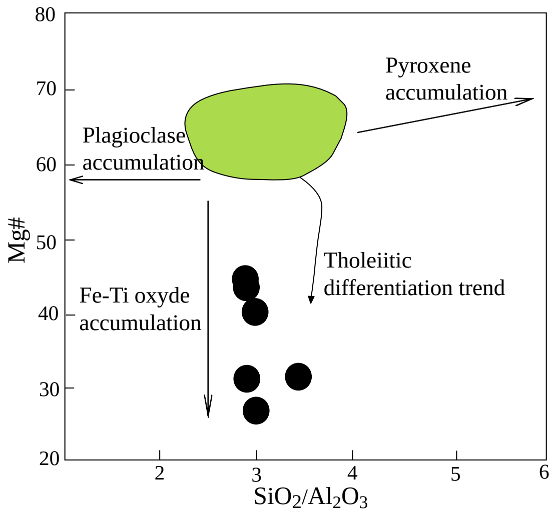

Figure 11. Mg# vs. SiO_2/Al_2O_3 diagram showing the primitive basalts field [55] and differentiation and mineral fractionation trends (after [56])

5.2. Age of protholith

From the Ar-Ar data, the flat cumulative patterns and the well-defined normal isochron of sample T21G9 means that sample were less disturbed, which is traduced by no significant loss or gain of Argon. The age of 547,50 ± 3,15 Ma may be correlated to an amphibolitic metamorphism phase related to the tectono-metamorphic events marking the end of Pan African orogeny. The important variation in the patterns of sample T22A, coupled to the fact that results are not defining an isochron, are the evidences of significant loss in Ar, this means samples were probably affected by multi phases metamorphism. The age of 618,14 ± 11,43 Ma yielded by T22A of the study area has been obtain by [15,23,57], (U-Pb / zircon age) [24,29,31,58,59,60]. The amphibolites are well documented in the CAFB in Cameroon during the Neoproterozoic [5,8,11,10,40]. [10] showed that amphibolites from the Yaoundé Group (Cameroon, Central Africa) have a basaltic affinity. They are dated between 650 and 600 Ma, and confirm the existence of a Neoproterozoic oceanic crust within the CAFB. The studied amphibolites are younger than the Makénéné amphibolites in the CAFB and the Mewongo amphibolites in the Congo craton which display an Archean age [5,7].

This age of 618 Ma traduces the local peak of metamorphism which is a high-grade amphibolite to granulite facies. At the regional scale this recurrent age of 618 Ma obtained by different method confirm that the Pan African Fold Belt in Cameroon is homogeneous regarding the ages of events. The Ar-Ar ages of the studied amphibolites characterize a polyphase metamorphism during the Pan African Orogeny in Banefo-Mvoutsaha.

5.3. Tectonic Setting and Geodynamic Implication

The Nb/Yb vs. Ba/Yb diagram [61] is useful to constrain the geodynamic settings of the protolith of the mafic metavolcanic rocks. According to this diagram, the studied amphibolites plot in the MORB array (Figure 12A), suggesting that the immobile trace element Nb could be used to separate the different types of ocean-floor basalts [62]. They are N-MORB related for the majority of samples, but they also display back arc basin basalts (BABB; Figure 12B) and Arc-Volcanic (Figure 12C) features. The protolith is alkali basalt, and alkali basalts often occur in a subduction area resulting from a collision between a continental and oceanic crusts [63]. The ternary MgO-$FeOT$-Al_2O_3 diagram of studied amphibolites after [64] displays a continental trend (Figure 13A). They are Continental Island Arc basalts, according to CaO-Na_2O-K_2O ternary plot of [65] (Figure 13B). On the others geotectonic discrimination diagrams that use immobile trace elements during metamorphism, all the samples belong to the same geotectonic setting which is intraplate context. This context is shown by the binary diagram Zr-Zr/Y of [66] in which the protoliths of studied amphibolites are intraplate basalts (Figure 14A). This is supported by the discrimination geotectonic Nb–Zr–Y [62] and the Th-Hf/3-Ta of [66] ternary diagrams. Indeed, the samples are plotted on AI and AII, which correspond to within plate alkali basalts and within plate tholeiitic basalts according to geochemistry results (Figure 14B). Furthermore, the Figure 14C confirms the same results.

6. Conclusion

From the petrography, the whole-rock geochemistry and Ar/Ar dating of the Banefo-Mvoutsaha amphibolites, the main findings are as follow:

1). Two distinct types of amphibolites outcrop in Banefo-Mvoutsaha area, the banded amphibolites and the massive amphibolites.

2). Both amphibolites are ortho-derived, their protoliths are alkali basalts which belong to tholeiitic series.

3). The studied samples are enriched in LREE relatively to HREE. The La_N/Yb_N ratios are between 5,78 and 8,03; and Gd_N/Yb_N values are from 1,39 to 1,85. The samples display a negative Eu anomaly with Eu/Eu* values comprised between 0,65 and 0,96. In general samples are enriched in LILE, and relatively weakly depleted in others elements.

4). The Ar/Ar geochronology reveals that all samples have Pan-African age. The banded amphibolites age is 618,14 ± 11,43 Ma and the massive amphibolites age is 547,50 ± 3,15 Ma. The older metamorphic event at 618 Ma match with the emplacement ages of granites that intruded the metamorphic basement of Banefo-Mvoutsaha area. The youngest metamorphic event at 547 Ma is related to the tectono-metamorphic events which mark the end of the Panafrican orogeny in the study area. Therefore, Panafrican orogeny in the study area presents multiphase metamorphism with at least two amphibolitic phases.

5). The Banefo-Mvoutsaha amphibolites are the volcanic input of a volcano-sedimentary protoliths of the metamorphic basement of the area. The massive and banded amphibolites are metabasites and have a basaltic composition. They are N-MORB related and display back arc basin basalts and Arc-Volcanic characteristics. They follow a continental arc trend and correspond to within plate alkali and within plate tholeiitic basalts.

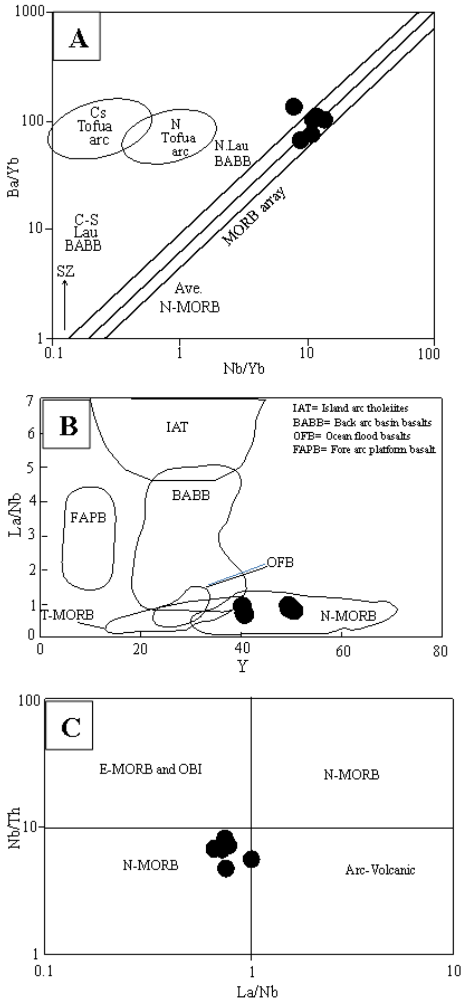

Figure 12. Tectonic setting discrimination diagrams of the Banefo-Mvoutsaha amphibolites. **A)** Nb/Yb vs. Ba/Yb diagram (after [61]). **B)** Y vs. La/Nb diagram showing the distribution of the main amphibolites within back-arc basin basalts (BABB) field, (after [67]). **C)** La/Nb vs. Nb/Th tectonic discrimination diagram showing the plots of the Penjween amphibolites within arc field, (after [68])

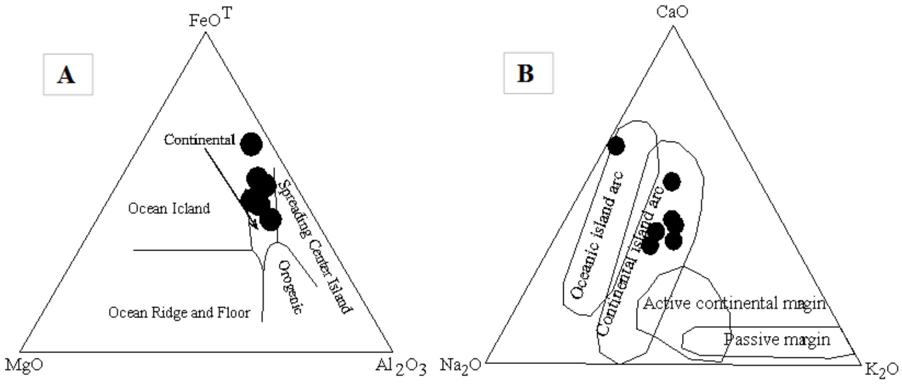

Figure 13. (A) MgO-FeOT-Al_2O_3 plot after [64]. **B)** CaO-Na_2O-K_2O ternary diagram showing sandstones compositions from oceanic Island Arc, Active Continental Margin tectonic settings [65]

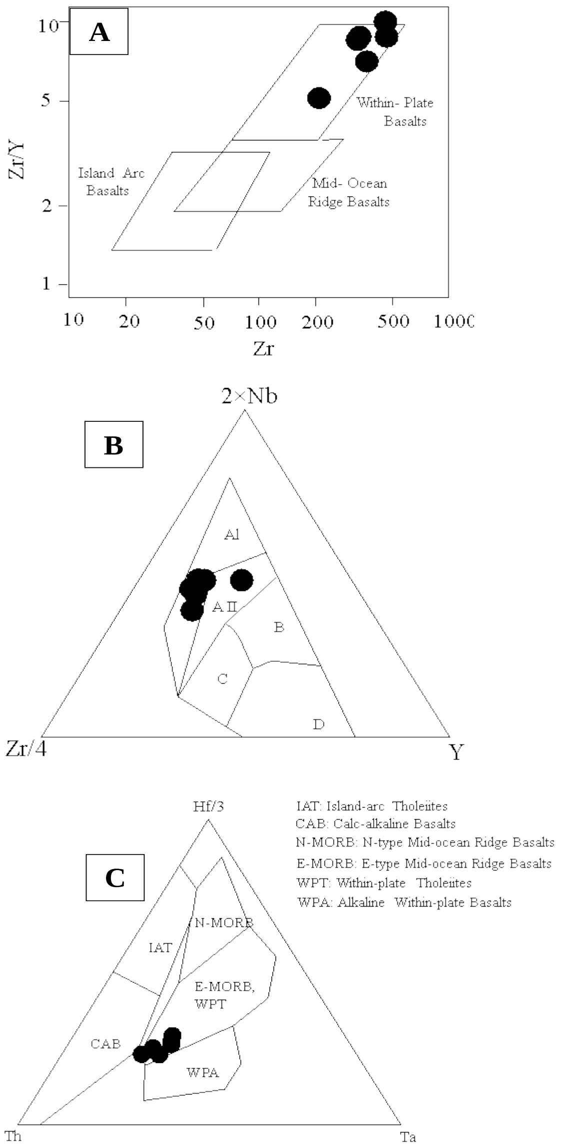

Figure 14. Geotectonic discrimination diagrams of the Banefo-Mvoutsaha amphibolites. **A)** Zr/Y vs Zr of [66] indicating geotectonic context of studied amphibolites. **B)** Nb–Zr–Y of [62]. WPA (AI, AII): Within-plate Alkalic Basalt; WPT (AII, C): Within-plate Tholeiitic Basalts; P MORB (B) plume mid-ocean ridge basalts; N MORB (D): normal mid-ocean ridge basalts; VAB (C, D): Volcanic Arc Basalts; WPB, Within-Plate Basalts; E-MORB, Enriched Mid-Ocean Ridge Basalts. **C)** Geotectonic diagram Th-Hf/3-Ta [69] showing the positions of Banefo-Mvoutsaha amphibolites within the WPT/WPA domain

ACKNOWLEDGEMENTS

The Ar-Ar geochronology presented here was possible through financial support and technical assistance of Prof Jan WIJBRANS from the Department of Isotope Geochemistry, Vrije Universiteit, de Boelelaan 1085, 1081HV Amsterdam, The Netherlands. We are grateful to Prof Jan WIJBRANS.

References

[1] Goodwin, A. M., 1991. Precambrian Geology. The Dynamic Evolution of the Continental Crust. *Academic Press.* Harcourt Brace Jovanovich Publishers 666 p.

[2] Shinjo, R., Chung, S.L., Kato, Y., et al., 1999. Geochemical and Sr-Nd isotopic characteristics of volcanic rocks from the Okinawa trough and Ryukyu arc: implications for the evolution of a young, intracontinental back arc basin. J. Geophys. Res. *Solid Earth* 104:10591–10608.

[3] Ernst, R.E., Buchan, K.L., 2001. Large mafic magmatic events through time and links to mantle plume heads. In: Ernst, R.E., Buchan, K.L. (Eds.), Mantle Plumes: Their Identification through Time. Special Paper *Geol. Soci. Am.* 352: 483–575.

[4] Harlan, S.S., Geissman, J.W., Snee, L.W., 2008. Paleomagnetism of Proterozoic mafic dikes from the tobacco root Mountains, Southwest Montana. *Precambrian Res.* 163: 239–264.

[5] Tchakounté, J., Eglinger, A., Toteu, S. F., Zeh, A., Nkoumbou C., Mvondo, O.J., … Barbey, P., 2017. The Adamawa-Yadé Domain, a piece of Archaean crust in the Neoproterozoic Central African Oro genic Belt (Bafia area, Cameroon). Precambrian Research, 299:210–229.

[6] Fossi, D.H., Dadjo Djomo, H., Takodjou Wambo, J.D., Ganno, S., Pour, A.B., Kankeu, B., Nzenti, J.P., 2021a. Structural lineament mapping in a sub-tropical region using Landsat-8/SRTM data: a case study of Deng-Deng area in Eastern Cameroon. *Arabian J. Geosci.* 14: 1–22.

[7] Kwamou, W.M.M., Nono, K., Nkouathio, G.D., Kenne, D.G.A., 2021. Petrogenesis and U-Pb zircon dating of amphibolite in the Mewengo iron deposit, Nyong series, Cameroon: fingerprints of iron depositional geotectonic setting. *Arab. J. Geosci.* 14:872

[8] Ganwa, A.A., Frisch, W., Siebel, W., Ekodeck, G. E., Shang, C. K., Ngako, V., 2008. Archean inheritances in the pyroxene–amphibole-bearing gneiss of the Méiganga area (Central North Cameroon): Geochemical and 207Pb/206Pb age imprints. *Compte Rendu Géosciences* 340: 211–222.

[9] Njanko, T., Nedelec, A., Affaton, P., 2006. Synkinematic high - K calc-alkaline plutons associated to the Pan-African Central Cameroon Shear Zone (W-Tibati area): Petrology and geodynamic significance. *Journal of African Earth Sciences* 44: 494-510.

[10] Owona S., Mvondo, O. J., Ekodeck G. E., 2013. Evidence of Quartz, Feldspar andAmphibole Crystal Plastic Deformations in the Paleoproterozoic Nyong Complex Shear Zones Under

Amphibolite to Granulite Conditions (West Central African Fold Belt, SW Cameroon). *Journal of Geography and Geology* 5:3.

[11] Fozing, E.M., Kwékama M., Gountié, D.M., Asobo N.E., Asaahd, Njankoa, T., Tcheumenak K.J., Efon, A.J., Njonfang, E., 2019. Petrography and geochemistry of amphibolites from the Fomopéa Pluton (West Cameroon): Origin and geodynamic setting. *Journal of african earth Science* 181–194.

[12] Kouankap Nono, G. D., NzentiJ. P., Suh C. E. and Ganno S., 2010. Geochemistry of ferriferous, high-K calc-alkaline granitoids from the Banefo-Mvoutsaha Massif (NE Bafoussam), Central Domain of the Pan-African Fold Belt, Cameroon. *The Open Geology Journal* 4: 15-28.

[13] Njiekak, G., Dörr, W., Tchouankoué, J. P. and Zulauf, G., 2008. “U-Pbzircon and microfabric data of (meta) granitoids of western Cameroon: constraints on the timing of pluton emplacement and deformation in the Pan-African belt of Central Africa”, *Lithos* 102: 460-477.

[14] Kouankap Nono, G.D., 2011. Etude du Cisaillement Centre Camerounais dans la région de Banefo-Mvoutsaha au NE Bafoussam, dans le domaine centre de la Chaine Panafricaine Nord Equatoriale: Petrogenèse, Géochronologie et Structurologie des formations du socle. Thèse de Doctorat / Ph. D, Université de Ydé I, 118 p.

[15] **Nzenti, J.P., Barbey, P., Macaudiere, J. and Soba, D., 1988.** Origin and evolution of late Precambrian high - grade Yaounde gneisses (Cameroon). Precambrian Research 38: 91 - 109.

[16] Davison, I., & Dos Santos, R. A., 1989.Tectonic Evolution of the Sergipano Fold Belt, NE Brazil, during the Brasiliano Orogeny. *Precambrian Research 45:* 319-342.

[17] Almeida, F.F.M., Hassui, Y., Brito de Neves, B.B., and Fuck, R., 1981. Brasiliano structural provinces: an introduction. *Earth Sciences Reviews* 17: 1-29.

[18] Castaing, C., Feybesse, J.L., Thiéblemont, D., Triboulet, C., and Chèvremont, P., 1994. Paleogeographical reconstructions of the Pan-African/Brasiliano orogen: closure of an ocean domain or intracontinental convergence between major blocks? *Precambrian Research* 69: 327-344.

[19] Brito neves, B.B., Van schmus, W.R., Fetter, A., 2002. North-Western Africa-North Estern Brazil: major tectonic links and correlation problems. *Journal of African Earth Sciences* 34: 275-278.

[20] Nzenti, J.P., Barbey, P., Bertrand, J.M. et Macaudiere, J., 1994. La chaine panafricaine au Cameroun: cherchons structures et modèles In S.G.F. édit. 15e, *réunion des Sciences de la terre*. France, 99 P.

[21] Nzenti, J.P., Kapajika, B., Wörner, G., and Lubala, R.T., 2006. “Synkinematic emplacement of granitoids in a Pan-African shear zone in Central Cameroon”. *J. Afr. Earth Sci.* 45:74-86.

[22] Nzenti, J.P., Njiosseu Tanko, E.L., Nzina, N. A., 2007. The metamorphic evolution of the Paleoproterozoic high grade Banyo gneisses (Adamawa, Cameroon, Central Africa). *J. Cam. Acad. Sci.* 7: 95–109.

[23] Ngnotué, T., Nzenti, J.P., Barbey, P and Tchoua, F.M., 2000. “The Ntui - Bétamba high-grade gneisses: a northward extension of the Pan- African Yaoundé gneisses in Cameroon”. *J. Afr. Earth Sci.* 31: 369-381.

[24] Tanko Njiosseu, E.L., Nzenti, J.P., Njanko, T., Kapajika, B. and Nédelec, A., 2005. “New U-Pb zircon ages from Tonga (Cameroon): coexisting Eburnean-Transamazonian (2.1 Ga) and Pan-African (0.6 Ga) imprints”. *C. R. Géosci.* 337: 551-562.

[25] Toteu, S.F., Michard, A., Bertrand, J.M. and Rocci, G., 1987. U/Pb dating of Precambrian rocks from northern Cameroon, orogenic evolution and chronology of the Panafrican belt in Central Africa. Precambrian Res. 37:71 - 87.

[26] Nédélec, A., Macaudière, J., Nzenti, J. P., et Barbey, P., 1986. Evolution structurale et métamorphisme des schistes de Mbalmayo (Cameroun). Informations pour la structure de la zone mobile panafricaine d'Afrique centrale au contact du craton du Congo. *Comptes Rendus Académie des Sciences*, Paris, 303: 75-80.

[27] Nzenti, J.P., 1998b. Neoproterozoic alkaline meta-igneous rocks from the Pan-African North Equatorial Fold Belt (Yaounde Cameroon): biotites and magnetite rich pyroxenites. Journal of African Earth Sciences 26: 37-47.

[28] Djouka-Fonkwé, M.L., Schulz, B., Schüssler, U., Tchouankoué, J-P. and Nzolang, C., 2008. Geochemistry of the Bafoussam Pan-African I- and S- type granitoids in western Cameroon. *J. Afr. Earth Sci.* 50: 148-167.

[29] Nzolang, C., Kagami, H., Nzenti, J.P. & Holtz, F., 2003. Geochemistry and preliminary Sr-Nd isotopic data on the neoproterozoïc granotoïds from the Bantoum area, West Cameroon: evidence for a derivation from a paleoproterozoic to Archean crust. Polar Geosciences, 16: 196-226.

[30] Nguiessi, T.C., Nzenti, J.P., Nsifa, E.N., Tempier, P. and Tchoua, F.M., 1997. “Les granitoïdes calco-alcalins, syncisaillement de Bandjadans la chaîne panafricaine nord-équatoriale au Cameroun”, *C. R. Acad. Sci.* 325: 95-101.

[31] Tagne-Kamga, G., Mercier, E., Rossy, M., Nsifa, N.E., 1999. Synkinematic emplacement of the Pan-African Ngondo igneous complex (west Cameroon, central Africa). *Journal of African Earth Sciences* 28: 675-691.

[32] Tagne-Kamga, G., 2003. Petrogenesis of neoproterozoic Ngondo plutonic complex (Cameroon West central Africa): a case of late collisional ferro-potassic magmatism. Journal of African Earth Sciences 36, 149-171.

[33] Tchaptchet Tchato, D., Schulz, B., Nzenti,J. P., 2009. Electron microprobe (EMP) monazite dating and P – T data of the Neoproterozoic metamorphic and mylonitic events in the Kekem area, Cameroon North Equatorial Fold belt. Neues Jahb. *Palaontol.* 186/1: 95-109.

[34] Qiu, H., and Wijbrans, J., 2006. Paleozoic ages and excess $_{40}$Ar in garnets from the Bixiling eclogite in Dabieshan, China: New insights from $_{40}$Ar / $_{39}$Ar dating by stepwise crushing. *Geochimica and cosmochimica.*

[35] Sun, S.S. and McDonough, W.F., 1989. Chemical and isotopic systematics of oceanic basalts: implications for mantle composition and processes. In: Saunders AD, Norry MJ (Eds.), Magmatism in the Ocean Basins. *Geological Society of London Special Publication* 42:313-345.

[36] Thompson, R.N., 1982, British Tertiary Volcanic province. Scott. *J. Geol.* 18: 49-107

[37] Winchester, J.A., Park, R.G. and Holland, J.G., 1980. The geochemistry of Lewisian semipelitic schists from the Gairloch District, wester Ross. *Scott. J. Geol.* 16, 165-179.

[38] Aye, B.A., Sababa, E., Ndjigui, P.D., 2017. Geochemistry of S, Cu, Ni, Cr and Au-PG from in the garnet amphibolites the Akom II area in the Archaean Cameroon. *Chem. de Erde* 77: 81–93.

[39] Evina Aboula, Y.S., Ndjigui, P-D., Mvondo Ondoa, J., 2023a. Petrology and geochemistry of metamorphosed rocks associated with iron formations of the Toko–Nlokeng iron deposit, (southern Cameroon): implications for geo dynamic evolution and mineralization. *Geol J.* 1–40.

[40] Winchester, J.A. and Floyd, P.A., 1977. Geochemical discrimination of different magma series and their differentiation products using immobile elements. Chem. Geol 20: pp. 325-343.

[41] Akihiko Fujiyama, 1992. Distinctive REE patterns for tholeiitic and calc-alkaline magma series co-occurring at Adatara colcano, Northeast Japan. *Geochemical jounal*, 26(6): 395-409.

[42] Jakes, P., and Gill J., 1970. Rare earth elements and the island arc tholeiitic series. *Science Direct* 9: 17-28.

[43] Kushiro, I., 1987. A petrological model of the mantle wedge and lower crust in the Japanese island arc. In B. O. Mysen, Ed., *Magmatic precesses: Physicochemical principles*, Special publication No 1, *The geochemical society*, University Perk, PA, 165-181.

[44] Perchuck, L.L., 1987. Studies of volcanic series related to the origin of some marginal see floors. In B.O. Mysen, Ed., Magmatic processes: Physicochemical Principles, Special publication No 1, *the geochemical society*, University Park, PA, 209-230.

[45] Bédard J.H., 2006. A catalytic delamination-driven model for coupled genesis of Archaean crust and sub-continental lithospheric mantle. *Geochim Cosmochim Acta* 70(5):1188–1214

[46] Rapp RP, Shimizu N, Norman MD (2003) Growth of early continental crust by partial melting of eclogite. Nature 425(6958):605.

[47] Pearce J.A., 1975. Basalt geochemistry used to investigate past tectonic environment in Cyprus. Tectonophysics. 25, 40-67

[48] Pearce J.A. and Cann J.R., 1973. Ophiolite origin investigated by discriminate analysis using Ti, Zr and Y. *Earth Planet Sci. Lett.* 12, 339-349.

[49] Abdel-Rahman, A.F.M. and P.E. Nassar, 2004. Cenozoic Volcanism in the Middle East: Petrogenesis of alkali basalts from Northern Lebanon. Geol. Mag., 140: 545-563.

[50] Moghazi, A.K.M., 2003. Geochemistry of a Tertiary Continental Basalt Suite, Red Sea Coastal Plain, Egypt: Petrogenesis and Characteristics of the Mantle Source Region. *Geological*

Magazine 140: 11-24.

[51] Wilson M., 1989. Igneous petrogenesis. Springer, London, 245–285.

[52] Hughes, C. J., 1973. Spilites, keratophyres and igneous spectrum. Geological Magazine, 109(6), 513–527.

[53] Irvine, T.N., Baragar, W.R.A., 2011. A guide to the chemical classifi cation of the Common volcanic rocks. *Can J. Earth Sci.* 8(5):158.

[54] Miyashiro, A., 1974. Volcanic rocks series in island arcs and active continental margins. Am J Sci 274, 321-355.

[55] Irvine, T.N. and Baragar, W.R.A., 1972. A Guide to the Chemical Classification of the Common Volcanic Rocks. Canadian Journal of Earth Sciences, 8, 523-548. http://dx.doi.org/10.1139/e71-055.

[56] Kempton, P.D., Harmon, R.S., 1992. Oxygen isotope evidence for large-scale hybridization of the lower crust during magmatic underplating. Sci Dir. *Geochemica and Cosmochemica* 56: 971 – 986.

[57] Ngnotué, T., Ganno, S., Nzenti Jean, P., Schulz, B., Tchaptchet Tchato, D.I., Suh Cheo, E., 2012. Geochemistry and Geochronology of Peraluminous High-K Granitic Leucosomes of Yaoundé Series (Cameroon): Evidence for a Unique Pan-African Magmatism and Melting Event in North Equatorial Fold Belt. *International Journal of Geosciences* 3, 525-548.

[58] Soba, D., 1989. La serie du lom: etude geologique et geochronologique d’un bassin volcano-sedimentaire de la chaine panafricaine à l’est du Cameroun, vol. 6. These de doctorat, Paris.

[59] Abaga, B., 1996. Les leucogranites et les orogènes, signification des leucogranites d'Akum (région de Bamenda, Nord-Ouest Cameroun) dans l'orogenèse panafricaine. Etude préliminaire. Mémoire Maîtrise, Université de Yaoundé I, 57p.

[60] Abaga, B., Nzenti, J. P., Njanko, T., Pedjui, P., Njiosseu, E. L. T., Nzolang, C., Kapajika, B., Mouangue, R. M., Tchoua, F. M., 1999. Le plutonisme peralumineux néoprotérozoïque, syntectonique dans la chaîne panafricaine nord-équatoriale du Cameroun. In: Vicat J.P. et Bilong P. (eds) Géologie et environnements au Cameroun. *Collection GEOCAM* 379 - 385.

[61] Pearce, J.A. and Stern, R.J., 2006. Origin of Back-Arc Basin Magmas: Trace Element and Isotope Perspectives. In: Christie, D.M., Fisher, C.R., Lee, S.M. and Givens, S., Eds., Back-Arc Spreading Systems; Geological, Biological, Chemical, and Physical Interactions. Geophysical Monograph Series 166, American Geophysical Union, Washington, 63-86.

[62] Meschede, M., 1986. A method of discriminating between different types of mid ocean ridge basalts and continental tholeiites with the Nb-Zr-Y diagram. *Chemical Geology* 56(3-4):207-218.

[63] Levinson, A. A., and Cook, F.A., 1994. Gem corundum in alkali basalt: origin and occurrence. *Gem and gemmology* 30(4): 253-262.

[64] Pearce T.H, Gorman B.E, Birkett T.C., 1977. The relationship between major element chemistry and tectonic environment of basic and intermediate volcanic rocks. *Earth Planet Sci. Lett.* 36:121–132

[65] Bhatia, M.R., 1983. Plate Tectonics and Geochemical Composition of Sandstone. *The Journal of Geology*, 91: 611-627.

[66] Pearce, J.A. and Norry, M.J., 1979. Petrogenetic implications of Ti, Zr, Y and Nb variations in volcanic rocks. Contrib. Mineral petrol 69: 33-47.

[67] Floyd P.A., Kelling G., Gökcen S.L. and Gökcen N., 1991. Geochemistry and tectonic environment of basaltic rocks from the Misis ophiolitic mélange, South Turkey. Chem. Geol., 89: 263-280.

[68] Thompson, R. N., Morrison, M. A., Hendry, G. L. & Parry, S. J. (1984). An assessment of the relative roles of crust and mantle in magma genesis: an elemental approach. Philosophical Transactions of the Royal Society of London A310, 549–590

[69] Wood, D.A., 1980. The application of a Th-Hf-Ta diagram to problems of tectono-magmatic classification and to establishing the nature of crustal contamination of basaltic lavas of the brutish tertiary volcanic province. *Earth Planet Sci. let.* 50: 11-30.

[70] Ross, P.S. and Bédard, J.H., 2009. Magmatic affinity of modern and ancient subalkaline volcanic rocks determined from trace-element discriminant diagrams. Canadian Journal of Earth Sciences, 46, 823–839.